Correlations Between the Same Motor Cortex Cells and Arm Muscles During a Trained Task, Free Behavior, and Natural Sleep in the Macaque Monkey

Andrew Jackson, Jaideep Mavoori and Eberhard E. Fetz

J Neurophysiol 97:360-374, 2007. First published Oct 4, 2006; doi:10.1152/jn.00710.2006

J Neurophysiol 97: 360–374, 2007.
First published October 4, 2006; doi:10.1152/jn.00710.2006.

Correlations Between the Same Motor Cortex Cells and Arm Muscles During a Trained Task, Free Behavior, and Natural Sleep in the Macaque Monkey

Andrew Jackson,[1] Jaideep Mavoori,[2] and Eberhard E. Fetz[1]

[1] *Department of Physiology and Biophysics and Washington National Primate Research Center and* [2]*Electrical Engineering, University of Washington, Seattle, Washington*

Submitted 11 July 2006; accepted in final form 29 September 2006

Jackson A, Mavoori J, Fetz EE. Correlations between the same motor cortex cells and arm muscles during a trained task, free behavior, and natural sleep in the macaque monkey. *J Neurophysiol* 97: 360–374, 2007. First published October 4, 2006; doi:10.1152/jn.00710.2006. Traditionally, the neural control of movement has been studied by recording cell activity in restrained animals performing repetitive, highly trained tasks within a restricted workspace. However, the degree to which results obtained under these conditions are valid during natural, unconstrained behavior remains unknown. Using an autonomous, implantable recording system, we examined the relationships between the firing of motor cortex cells and forearm muscle activity in primates under three behavioral conditions: performance of a conventional torque-tracking task, unrestrained behavior, and natural sleep. We found strong correlations over long periods of daytime activity, suggesting a consistent relationship between cortex and muscles across the repertoire of awake behavior. The range of correlation values was comparable during task performance, but many individual cells exhibited significant differences across conditions. During the night, phases of sleep were associated with a cyclical pattern of cell and muscle activity. Across the population, the strength of cell-muscle correlations was related to preferred direction for daytime but not nighttime activity. The relationship of cells to behavior remained consistent over periods of several weeks. These findings extend the interpretation of results obtained under constrained conditions and are relevant to the development of neural prostheses for restoring natural movements to patients with motor deficits.

INTRODUCTION

Since the pioneering work of Evarts (1964), extracellular recordings of action potentials in awake primates have greatly advanced our understanding of the neural control of movement and may eventually lead to the development of neural prostheses for patients with motor deficits (Donoghue 2002). The firing rate of motor cortex cells has been related to a variety of movement parameters including direction (Georgopoulos et al. 1982), force (Cheney and Fetz 1980; Evarts 1968), velocity (Moran and Schwartz 1999), final posture (Aflalo and Graziano 2006), muscle activity (Holdefer and Miller 2002; McKiernan et al. 1998; Townsend et al. 2006), and combinations of these (Thach 1978). However, the traditional techniques for sensing, amplifying, and recording action potentials have limited previous studies to artificially constrained behavior. Typically animals sit in a chair, often with head position fixed and limbs restrained, performing highly trained, stereotyped movements within a restricted workspace. Moveable microelectrodes advanced into the cortex are connected with cables to large, rack-mounted amplifiers and recording equipment (Lemon 1984).

Constrained experimental paradigms offer the methodological advantage of controlled movements under conditions that can be systematically varied but may be unrepresentative of natural behavior. Furthermore, stereotyped motion imposes correlations between movement parameters, which could lead to spurious relationships being mistaken for neural coding (Fetz 1992; Todorov 2000). For example, the directional tuning of cell activity calculated for movements from a single arm position does not generalize to the entire range of motion (Aflalo and Graziano 2006; Caminiti et al. 1990). Moreover, repetition may influence the representation of trained actions (Nudo et al. 1996). Therefore it remains to be seen how generally applicable results obtained under these experimental conditions are to natural, unconstrained behavior.

Advances in chronic recording electrode techniques (Hoogerwerf and Wise 1994; Kralik et al. 2001; Nordhausen et al. 1996) and autonomous, implantable electronics (Jackson et al. 2006a; Mavoori et al. 2005) are for the first time allowing continuous single-unit recording in completely unrestrained primates. In contrast to repetitive tasks, an unconstrained paradigm allows the study of natural, synergistic motor control. With an implanted recording system, the same cells can be followed long-term and related to movements through the entire repertoire of normal behavior including sleep states as well as task performance. Although unconstrained behavior is difficult to quantify and may not sample the movement space systematically, experiments in freely behaving animals are essential for understanding the neural control of natural movements and provide information crucial to the informed development of neuromotor prostheses (Jackson et al. 2006a,b).

Using a novel implanted recording system, we have for the first time contrasted activity obtained during constrained and unconstrained paradigms. We recorded the firing rate of the same primary motor cortex (M1) cells during performance of a trained motor task, unrestrained behavior, and natural sleep with the aim of determining how results obtained under constrained conditions generalize to completely unrestrained behavior. Motor activity was characterized by muscle electromyogram (EMG), which provides a simple and consistent quantification that can be compared across conditions. We found robust correlations between cortical cells and EMG on a variety of time scales during each condition. In particular, high correlation coefficients between M1 firing rates and EMG

Address for reprint requests and other correspondence: E. Fetz, Dept. of Physiology and Biophysics, University of Washington, 1959 NE Pacific St., Seattle, WA 98195-7290 (E-mail: fetz@u.washington.edu).

The costs of publication of this article were defrayed in part by the payment of page charges. The article must therefore be hereby marked "*advertisement*" in accordance with 18 U.S.C. Section 1734 solely to indicate this fact.

profiles over up to seven hours of unrestrained daytime activity suggests a largely consistent muscle representation across the behavioral repertoire. However, the cell-muscle correlations obtained for free behavior often differed from those during task performance; some cells exhibited strikingly different patterns in each condition. Nevertheless, for the population of cells we could relate the average strength of cell-muscle correlations during free behavior to the preferred direction of the cell as defined from the trained task. During the night, motor cortex cells exhibited a cyclical pattern reflecting rapid-eye-movement (REM) and slow-wave sleep phases with bursts of muscle activity observed predominantly at the beginning and end of REM sleep. The pattern of cell-muscle correlation during this period differed from daytime recordings and no longer reflected directional preference in the task. Some of these results have been published previously in abstract form (Jackson et al. 2005).

METHODS

Behavioral training

Two male *Macacca nemestrina* monkeys (*monkey Y*: 3 yr, weight: 4.3 kg, and *monkey K*: 3 yr, weight: 4.6 kg) were trained to perform a two-dimensional torque-tracking task with the right wrist. The monkeys sat in a chair with the elbow and hand immobilized by padded restraints. A six-axis force transducer (model FS6, AMTI, Watertown, MA) measured the isometric torque exerted by the monkeys around the wrist joint, and the flexion-extension and radial-ulnar components of this torque controlled the horizontal and vertical position of a cursor on a screen. The monkey's task was to hold the cursor inside targets which appeared on the screen. One complete trial required the monkey to move the cursor from a central target to one of eight peripheral targets and hold for 1 s before returning to the center to receive a fruit sauce reward.

Surgical implants

Before surgery, an array incorporating 12 microwire electrodes was assembled under sterile conditions using 50-μm-diam, Teflon-insulated tungsten wire (No. 795500, A-M Systems, Carlsborg, WA) cut flush with sharp scissors, yielding a tip impedance of around 0.5 MΩ at 1 kHz. The wires ran from a crimp-connector (Centi-Loc, ITT Canon, Santa Ana, CA) into polyamide guide-tubes ~20 mm in length which funneled into a 6 $\times$ 2 array (inter-electrode spacing: 500 μm). Each guide tube was filled with ophthalmic antibiotic ointment (Gentak, Akorn, Buffalo Grove, IL) and sealed at both ends with silastic (Kwik-Sil, WPI, Sarasota, FL).

The monkeys received pre- and postoperative corticosteroids (dexamethasone: 1 mg/kg po) to reduce cerebral edema. During a surgery performed under inhalation anesthesia (isoflurane: 2–2.5% in 50:50 O_2:N_2O) and aseptic conditions, the scalp was resected and a craniotomy made over left M1 (A: 13 mm, L: 18 mm). The dura mater was removed, and the pia mater was bonded to the edge of the craniotomy with cyano-acrylate glue to prevent cerebrospinal fluid leakage and to stabilize recordings (Kralik et al. 2001). The central sulcus was visualized, and the precentral cortex was stimulated with a silver ball electrode to locate the lowest threshold site for eliciting wrist and hand movements. The microwire assembly was positioned at this location with the long axis of the array running parallel to the central sulcus, and the connector was anchored with dental acrylic to several titanium skull screws. Because the Teflon-insulated microwires slide freely through the silastic seal, our design allowed each wire to be lowered individually into the cortex during surgery and adjusted at any time subsequent to implantation.

A 6-cm-diam cylindrical titanium chamber to protect the microwire assembly and house the electronics was anchored with additional skull-screws. Wires were wrapped around two of the screws to serve as ground connections. Any remaining space inside the craniotomy was filled with gelfoam, and the exposed skull was coated with dental varnish (Copaliner, Bosworth, East Providence, RI). The inside of the implant was sealed with a thin layer of dental acrylic covering the skull and craniotomy. The casing was closed with a removable Plexiglas lid, and the skin was drawn around the implant with sutures. Twisted pairs of stainless steel wires were tunneled subcutaneously from the inside of the casing to a connector on the monkey's back for attaching EMG electrodes. Surgery was followed by a full program of analgesic (buprenorphine: 0.15 mg/kg im and ketoprofen: 5 mg/kg po) and antibiotic (cephalexin: 25 mg/kg po) treatment.

During the course of the experiment, the monkeys were lightly sedated with ketamine (10 mg/kg im) on a weekly basis to sterilize the inside of the head casing (with dilute chlorohexadine solution followed by alcohol). With the monkeys sedated, the cortical microwires could be moved to sample new cells. This was usually performed every 2–3 wk and always after the interior of the casing had been sterilized. The microwires were moved by grasping the loop of exposed wire between the connector and guide-tube with sterile forceps. Typically, four to eight wires were adjusted sequentially while monitoring the recorded signal for action potentials. We concentrated on moving the wires into the approximate vicinity of cell activity rather than trying to optimize for specific units because cells obtained immediately after moving the wires proved to be unstable as the tissue settled. Often different units appeared over the course of the next day, including on wires which had been initially quiet. Typically this procedure resulted in 1 to 5 securely isolated single units 1 day after moving the wires; these units could then be recorded stably for several days to weeks.

While the monkeys were sedated, EMG electrodes made from pairs of braided steel wire (No. A5637, Cooner Wire, Chatsworth, CA) with 2–3 mm of insulation stripped from the end were inserted transcutaneously into various arm and wrist muscles using a 22-gauge needle. Electrode pairs were spaced ~1 cm apart. The leads were fixed to the skin with a drop of cyano-acrylate glue, covered with surgical tape and plugged into the back connector. Throughout the experiment the monkeys wore loose-fitting, long-sleeved jackets to protect the wires and back connector.

All procedures were approved by the University of Washington Institutional Animal Care and Use Committee (IACUC).

Neurochip electronics

A detailed description of our Neurochip Brain-Computer Interface system has been published previously (Jackson et al. 2006a; Mavoori et al. 2005). The complete implant, including circuit boards and 3.6 V lithium battery is shown in Fig. 1*A*. The electronics are designed around two mixed-signal processors that operate in parallel; each processor is a Programmable System on a Chip (PSoC, Cypress Semiconductor, San Jose, CA). The primary PSoC samples unit data from one cortical microwire at 11.7 ksp/s and handles infrared (IR) communication with a desktop computer. A second PSoC multiplexes and samples up to two differential, rectified EMG signals at 2 ksp/s per channel. An asynchronous serial bus synchronizes recordings and relays data between PSoCs. Front-end signal processing includes band-pass filtering and amplification (for neural signals: 500 Hz to 5 kHz, 1,500 times with a further 1–48 times variable gain; for EMG: 20 Hz to 2 kHz, 250 times with further 1–48 times followed by full-wave rectification). Each PSoC incorporates an 8-bit microprocessor core for digital processing (including spike discrimination and EMG averaging) and can store data to independent 8 Mb nonvolatile memory chips.

The Neurochip has three modes of operation, which are selected via IR commands. In the first mode, neural and EMG signals were recorded

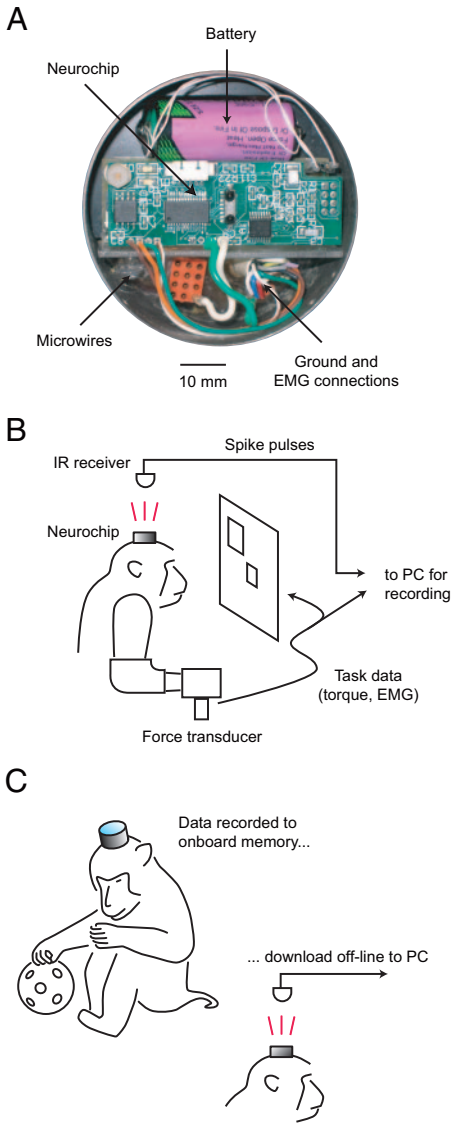

FIG. 1. The Neurochip system for neural and muscle recording during free behavior. *A*: head implant containing circuit boards, battery, microwire electrodes and connector for electromyographic (EMG) signals. *B*: during the trained task, the Neurochip detected spikes and transmitted pulses via infrared (IR). Task data and EMG signals were recorded via conventional laboratory instrumentation. *C*: during free behavior, neural and EMG signals were recorded to on-board memory. The data were subsequently downloaded off-line via IR.

directly to on-board memory and downloaded off-line via IR. In this mode, the memory can hold 90 s of raw neural data and two channels of rectified EMG data. The raw neural recordings were used to identify action potentials off-line and choose appropriate spike discriminator settings. In the second mode, used while the monkey performed the trained task (Fig. 1*B*), the Neurochip detected action potentials in real time using a window discriminator algorithm. The Neurochip produced a brief IR flash whenever the neural signal crossed a threshold level and subsequently passed through two adjustable time-amplitude windows. An IR receiver positioned above the monkey's head detected the flashes, while EMG was band-pass filtered (20 Hz to 5 kHz) and amplified (1,000–5,000×) using conventional laboratory instrumentation (MCP, Alpha-Omega Engineering, Nazareth, Israel). A PC equipped with a data-acquisition card (DAP 3200a, Microstar Laboratories, Bellevue, WA) recorded the spike and task events at 25 ksp/s, and EMG and torque signals at 5 ksp/s.

For extended recording during completely unrestrained behavior, the Neurochip operated in a third mode (Fig. 1*C*). The primary PSoC calculated and stored the spike count over consecutive time bins, whereas the secondary PSoC recorded average rectified EMG level over the same bins. Short sections of raw data were interleaved with the binned data to check recording and discrimination quality. The data reported here were recorded with 100-ms bins with each 3-min section of binned data interleaved with 22 ms of raw recording. In this configuration the Neurochip can store 26 h of continuous neural recording with one EMG channel or 13 h of recording with two EMG channels.

Data analysis

The relationship between neural and muscle activity during free behavior was characterized using cross-correlation functions (CCFs). We calculated the linear correlation coefficient, r, between the binned spike rate and mean rectified EMG shifted either forward or backwards by time, Δ, from -100 to $+100$ s (positive time-lags indicate the neural signal leading the muscle signal). These calculations were performed over the entire record of 100-ms bins, so a CCF based on 6 h of data reflects the correlation between 216,000 pairs of data values. In many cases, we found that features in the CCFs were well fitted by the sum of two Gaussian curves given by the following expression

$$r(\Delta) = A_1 e^{-(\Delta - t_1)^2/w_1^2} + A_2 e^{-(\Delta - t_2)^2/w_2^2} + A_3 \quad (1)$$

Least-squares fitting was performed using an iterative simplex search method (function *fminsearch*, MatLab, Mathworks, Natick, MA). The optimized fit coefficients were used to quantify for each component the amplitude, A_i, and half-width at half-maximum, HW_i, given by

$$HW_i = w_i \sqrt{\ln(2)} \quad (2)$$

To assess the significance of CCF features, we constructed 100 shuffled datasets from 1-min sections of the same data and performed equivalent correlation analysis. The 95% range of r values obtained from these uncorrelated datasets was used to construct confidence limits for significant CCF peaks and troughs. Correlation analysis assessed the degree to which observed EMG could be described by a fixed, linear function of cell firing rate. For some cells, we compared this to a model in which the linear fit parameters were allowed to vary over 10- or 1-min sections. Parameters were chosen to minimize the mean squared error between modeled and observed EMG within each section separately. The correlation coefficient between modeled and observed EMG was then calculated over the entire record.

Cell tuning during the torque-tracking task was determined from peri-event time histograms (PETHs) of spike activity aligned to the end of the hold period for each of the eight torque directions. A one-factor ANOVA assessed the effect of direction on the number of spikes occurring during each one-second hold period. For cells with a significant ($P < 0.05$) directional tuning, a preferred direction vector was calculated by summing each torque direction vector, weighted by the mean firing rate during the hold period for that direction. CCFs for the task condition were compiled from data recorded through our laboratory instrumentation. These data were first converted into firing rate and mean rectified EMG over consecutive 100-ms bins comparable with data recorded by the Neurochip. Although the filter cut-off and gain used with the laboratory instrumentation differs slightly from the Neurochip front-end configuration, this is unlikely to influence our results since the majority of the EMG spectral power is <1,000 Hz and our results were expressed as correlation coefficients normalized within the range -1 to $+1$. To further ensure that differences in recording method used in each condition did not influence our results, some cell-muscle pairs were recorded during the task using first the

laboratory instrumentation and then the Neurochip. CCFs compiled from both datasets exhibited equivalent features.

RESULTS

Dataset

The analysis presented here is based on 45 cells (16 from *monkey K,* 29 from *monkey Y*), recorded during daytime free behavior for an average of 4.9 h (range: 30 min to 11 h), and during the night time for an average of 7.7 h (range: 4–12 h). Analysis of task-related activity was based on sections of recording comprising ≥10 successful trials for each of the eight directions. No postspike effects from these cells were observed in spike-triggered averages of recorded EMG.

Long-term neural and muscle recordings during natural behavior and sleep

Figure 2*A* shows a 20-s section of raw signal recorded by the Neurochip from a microwire in the hand area of M1 while the monkey reached for food rewards presented by the experimenter. The recording shows bursts of action potentials, coinciding with activation of wrist muscles revealed in rectified EMG signals (Fig. 2*B*) recorded simultaneously from extensor carpi radialis (ECR) and flexor carpi ulnaris (FCU). The raw recording was used to select appropriate discriminator window settings prior to a longer period of data collection. Figure 2*C* shows the waveforms accepted by the Neurochip's dual time-amplitude window discriminator. To ensure that these waveforms represented action potentials from a single neuron, we compiled an interspike interval (ISI) histogram based on 90 s of recording (Fig. 2*D*). The unimodal ISI distribution is characteristic of a single unit and the absence of intervals shorter than the typical refractory period of a cortical neuron (~1 ms) indicated that only one cell generated the accepted spikes (Fig. 2*E*).

Figure 3*A* shows activity of the same cell and muscles recorded by the Neurochip over a 13-h period of unrestrained behavior in the cage beginning at 12:45 pm. Sample spike waveforms extracted from the interspersed raw data are shown above the plot. During the daytime, muscle activity was generally high as the monkey foraged for food, played with toys, and walked or swung around the cage. During the night, muscles were largely inactive, except for sporadic bursts of EMG. For display purposes, the data here are plotted as average firing rate and mean rectified EMG over consecutive 1-min intervals, but the original data were stored using 100-ms bins throughout the entire record. Figure 3, *B* and *C,* plots sample 1-min sections from the day and nighttime at the 100-ms time resolution, showing peak firing rates during individual bins exceeding 100 Hz.

Cross-correlation functions between neural and muscle activity

To characterize the relationship between motor cortex cell and muscle activity during free behavior, we compiled CCFs between firing rate and rectified EMG over 100-ms bins for the separate periods of day- and nighttime recording (see METHODS). During the day, this cell exhibited a positive correlation peak of 0.30 at zero lag with muscle ECR (Fig. 4*A*). A narrow

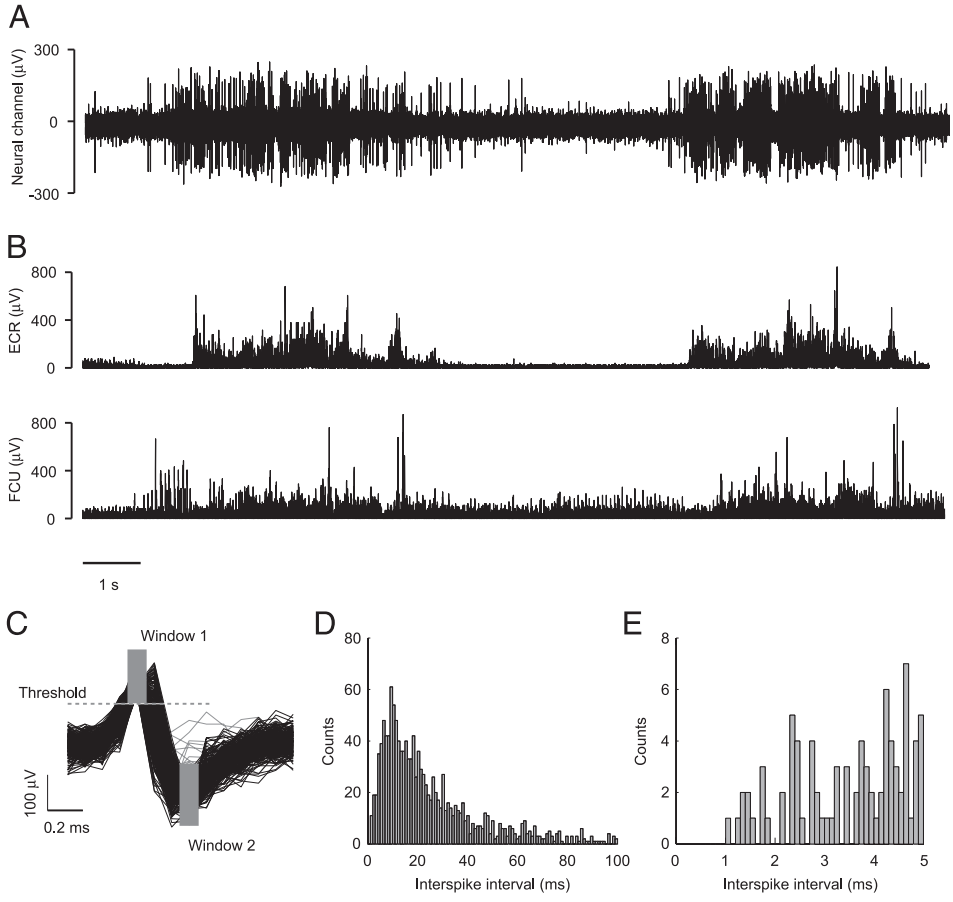

FIG. 2. Raw recording with the Neurochip. *A*: signal recorded by the Neurochip from a microwire electrode in primary motor cortex (M1) while *monkey K* reached for food. *B*: simultaneous recording of rectified EMG activity from wrist muscles extensor carpi radialis (ECR) and flexor carpi ulnaris (FCU). *C*: action potential waveforms from this recording that were accepted by the Neurochip's dual time-amplitude window discrimination algorithm. Rejected waveforms are shown in gray. *D*: interspike interval (ISI) histogram for spikes discriminated from 90 s of recording. The unimodal distribution is characteristic of a single cortical cell. *E*: ISI histogram with expanded time base shows an absence of short intervals <1 ms, the refractory period of a single unit (and longer than the discriminator refractory time of 0.5 ms).

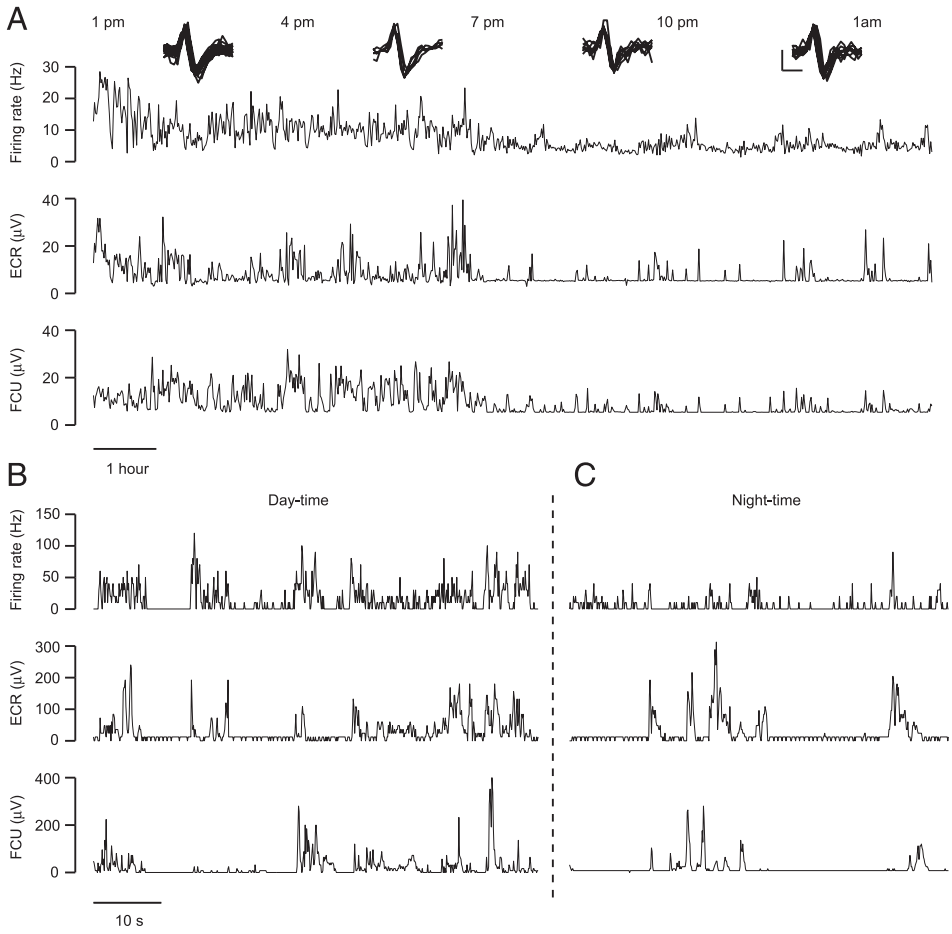

FIG. 3. Continuous, long-term recording with the Neurochip. *A*: continuous record of 13 h of spike firing rate and mean rectified EMG from *monkey K*. For clarity, mean values over consecutive 1-min bins are plotted, although the Neurochip stores data over 100-ms bins. Superimposed action potential waveforms were taken from the raw data sampled throughout the recording period (scale bars: 100 μA, 0.5 ms). *B*: section of the daytime record plotted at 100-ms resolution. *C*: section of the nighttime record plotted at 100-ms resolution.

negative correlation trough of −0.02 was seen with FCU (cortex leading the muscle by 1 100-ms bin). These features were both superimposed on broader peaks that reflected positive correlation on the time scale of behavioral episodes during which average cell and muscle activity was elevated. The narrow peak or trough indicates a more precise temporal relationship between cell and muscle within each episode and may reflect direct or indirect descending control from motor cortex. Activity during the night showed a different pattern of CCFs with the cell positively correlated with both muscles

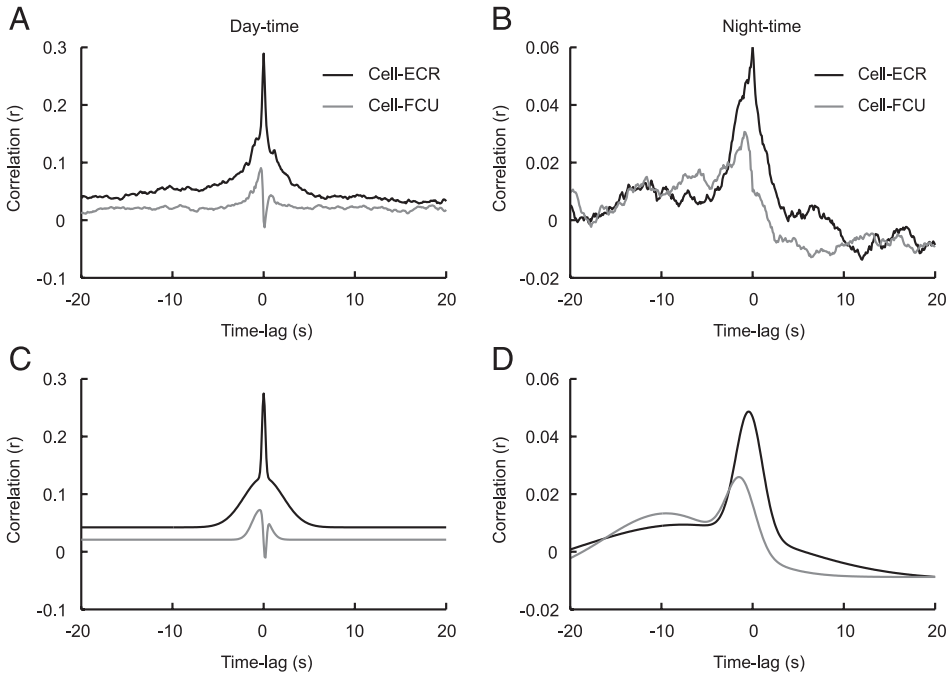

FIG. 4. Cross-correlation functions (CCFs) between cell's firing rate and rectified EMG. *A*: CCFs between firing rate and ECU and FCU over 6 h of daytime recording (12:45–6:45 pm). *B*: CCFs calculated for 6 h of nighttime recording (7:30 pm to 1:30 am). *C* and *D*: double Gaussian fits of CCFs in *A* and *B*.

(Fig. 4*B;* ECR: 0.06, FCU: 0.03). To quantify and compare CCFs, these features were fitted by a sum of two Gaussian components (see METHODS), shown in Fig. 4, *C* and *D*.

To examine the stability of cell-muscle relationships throughout the recording, we compared CCFs calculated over the entire record with CCFs for shorter sections of data. Figure 5,*A* and *B* shows the CCF for 6 h of daytime recording and average CCFs calculated using nonoverlapping 10- and 1-min sections of the same data. The narrow peak is very consistent throughout, although the broad peak is slightly attenuated for shorter windows. The gray shading indicates 95% confidence limits obtained from shuffled versions of the same 1-min sections, demonstrating that these cross-correlation features are larger than could be expected to arise by chance. The dark line in Fig. 5*C* plots the zero-lag correlation coefficient between cell firing and muscle ECR calculated over consecutive 10-min intervals through 12 h of day- and nighttime recording. During the daytime, the correlation between cell activity and this muscle remained positive and approximately constant. The gray shading indicates the range of correlation coefficients obtained for shorter 1-min sections within each 10-min interval. For some 1-min sections the value is close to zero. However, inspection of the data indicated that this was due primarily to periods during which the muscle was inactive. During the night, the correlation is generally low because the muscle is predominantly quiet, although sporadic nighttime EMG activity is associated with occasional periods of positive correlation.

The similarity of correlation coefficients calculated over different windows during the daytime implies a consistent linear relationship between cell firing rate and EMG activity. To test this further, we examined the degree to which the linear correlation between cell and EMG activity was improved by allowing the fit parameters to vary over 10- and 1-min intervals (see METHODS). This effectively increases the number of model parameters and inevitably leads to a better approximation of the observed data. However, if the cell-muscle relationship is constant throughout, allowing these parameters to vary should yield only modest improvements to the regression coefficient. Figure 5*D* shows the result of this analysis for the day- and nighttime separately. For the daytime data, fitting over 10- and 1-min sections produced little improvement, yielding correlation coefficients of 0.34 and 0.43, respectively, compared with 0.30 when the relationship was assumed to be fixed throughout. Varying the fit parameters had more effect on the correlation during the nighttime, which increased from 0.06 to 0.31 for shorter intervals. We repeated this analysis for 10 cell-muscle pairs showing strong daytime correlation with similar results (Fig. 5*E*). Thus it appears that the firing rate of some cells exhibits a consistent relationship with muscles thoughout unconstrained daytime behavior but that during the night, this relationship is more variable. The reason for this variability is explored in the next section.

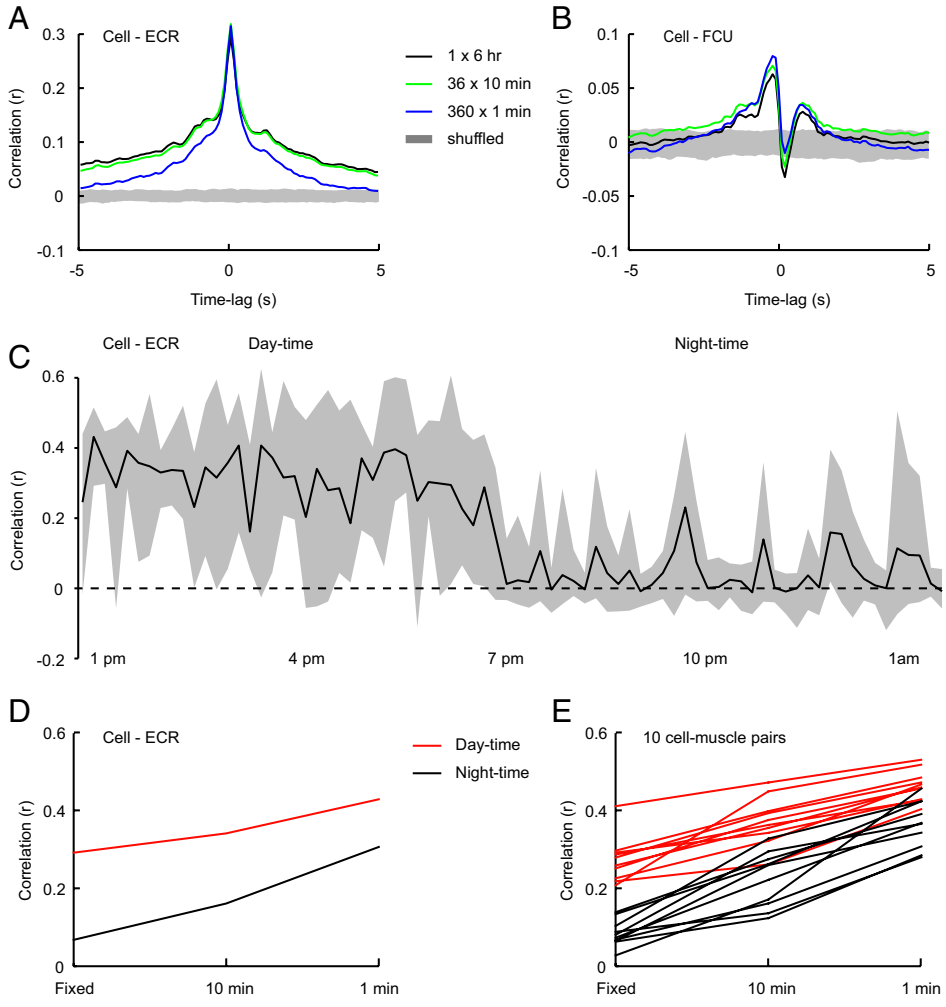

FIG. 5. Effects of window length on CCFs. *A*: CCF calculated for a 6-h daytime recording of cell firing and rectified ECR activity (black line). Also shown is the average CCF for nonoverlapping 10-min (green line) and 1-min (blue line) sections of the same data. Gray shading indicates the 95% range of CCFs compiled from data comprising the shuffled concatenations of the same 1-min sections. *B*: equivalent plot for CCFs compiled with muscle FCU. *C*: 0-lag cell-ECR correlation coefficient calculated for consecutive 10-min sections through 13 h of day- and nighttime activity. Gray shading indicates maximum and minimum values from corresponding 1-min sections. *D*: correlation between ECR activity and a linear model of cell firing rate in which the parameters are fixed, or allowed to vary over 10- and 1-min sections. Data from 6 h of daytime recording (12:45–6:45 pm) and 6 h of nighttime recording (7:30 pm to 1:30 am) fit separately. *E*: comparable plots for 10 different cell-EMG pairs.

Sleep cycles and movements during nighttime recordings

During the night, M1 cells exhibited a cyclical pattern of quiescence interspersed by periods of elevated activity, with one complete cycle lasting 40–60 min (Fig. 6*A;* mean firing rate and EMG calculated over 1-min bins). Bursts of EMG were seen predominantly at the onset and/or near the end of each period of elevated cortical activity and were correlated with cell firing rate. However, during the period of highest cortical firing, muscle activity was completely suppressed. Figure 6*B* shows an expanded record of firing rate and EMG for 100-ms bins during a typical cycle of elevated cortical activity. Across 8 h of nighttime recording this cell had a mean nighttime firing rate of 12 Hz, only slightly lower than for the daytime activity (16 Hz). Peak firing rates during the cyclical periods of elevated activity often exceeded 100 Hz. For this cell-muscle pair, the CCF showed periodic peaks corresponding to the time course of sleep cycles (Fig. 6*C*). The peak correlation of 0.13 was lower than that during the day (0.18; data not shown), but this value is low in part because the muscles were often silent during the periods of highest cortical activity. The CCF compiled specifically for only those minutes during which the muscle was co-activated had a higher correlation peak of 0.30 (Fig. 6*D*).

Video recording revealed that nighttime muscle activity corresponded with episodes of limb twitching, scratching, postural adjustments, and apparent waking behavior. However, unlike during the daytime, correlations between cells and muscles were always positive during these episodes. Even CCFs compiled with ipsilateral muscles exhibited correlation peaks. Figure 6, *E* and *F,* shows CCFs between a cell in left M1 and EMG recorded from muscle FCR of the right (contralateral) and left (ipsilateral) arm. During the daytime (Fig. 6*E*), there was a strong correlation peak with the contralateral muscle but a flat CCF with the ipsilateral muscle. By contrast, during the night CCFs with both contra- and ipsilateral muscles displayed positive peaks (Fig. 6*F*).

Summary of CCF features during day- and nighttime

The parameters of the CCFs obtained for day- and nighttime activity for all cell-muscle pairs are shown in Fig. 7 (*left* and *right*). Figure 7*A* summarizes the maximum (minimum) correlation value for the central peak or trough in 85 daytime CCFs

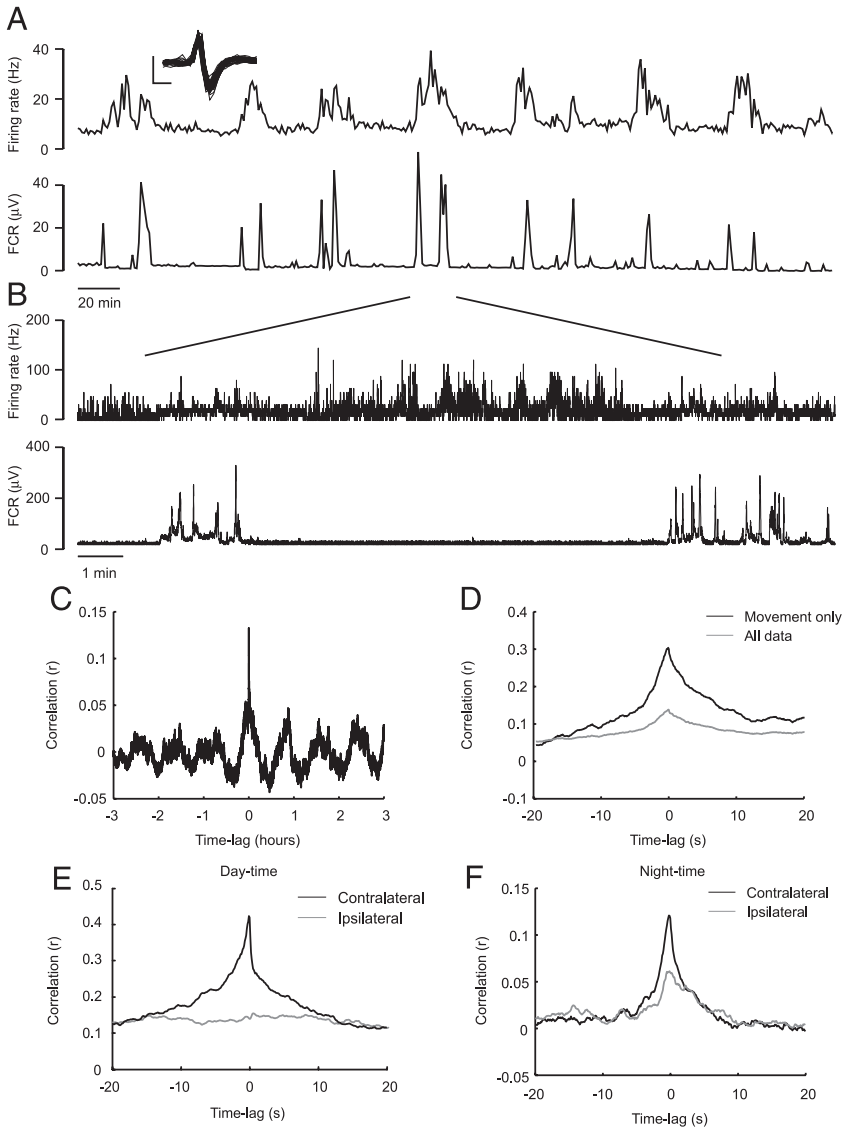

FIG. 6. Sleep cycles in motor cortex. *A*: average cell firing rate and rectified EMG from muscle ECR over 1-min bins during 6 h of nighttime recording showing cycles of slow-wave and rapid-eye-movement (REM) sleep. Sample spike waveforms for this cell are *inset* (scale bars: 500 μV, 0.2 ms; *monkey Y*). *B*: expanded plot of 1 sleep cycle plotted at 100-ms time resolution. *C*: CCF between cell and muscle activity plotted over an extended time scale. *D*: same CCF on shorter time scales calculated for all the data and for only those 1-min periods accompanied by muscle activation. *E*: CCF calculated for contralateral and ipsilateral FCR muscle during 3 h of daytime free behavior. *F*: equivalent CCFs for 9 h of nighttime activity.

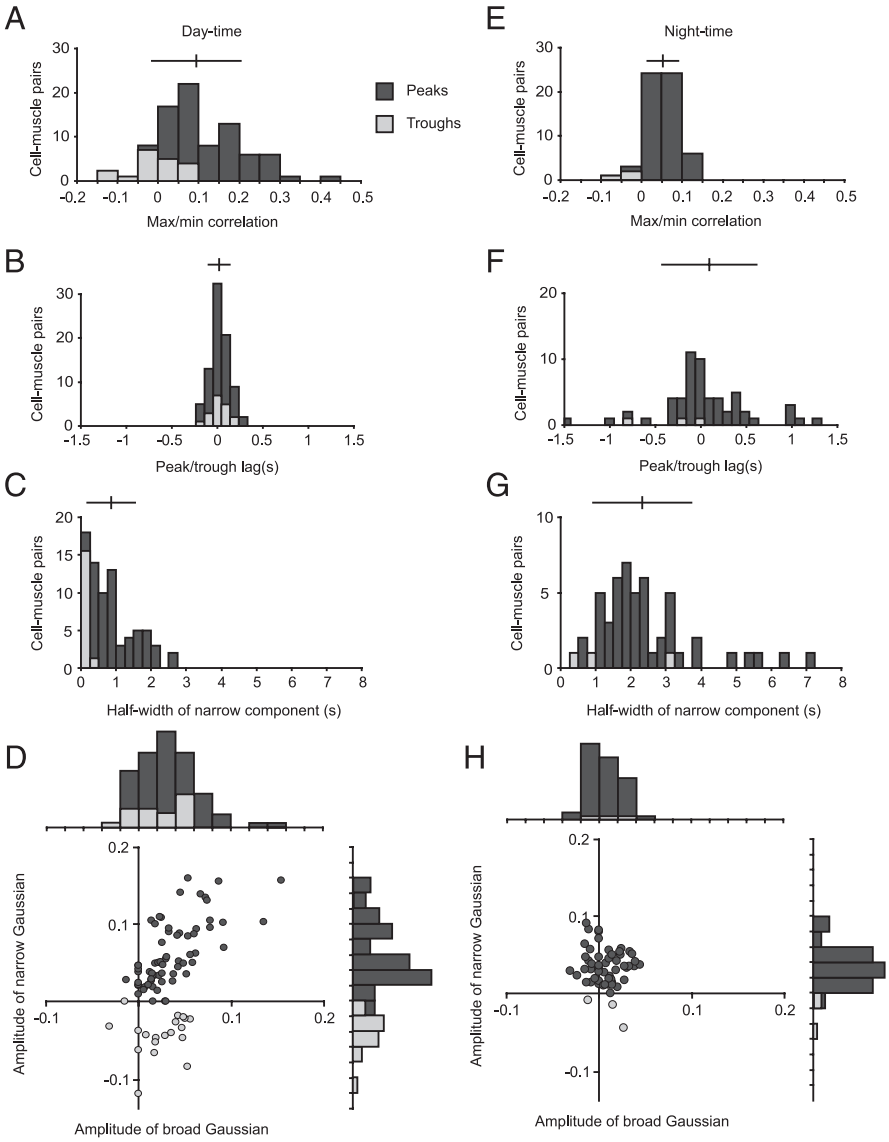

FIG. 7. Summary of CCF features during day- and nighttime activity. *A*: histogram of amplitude of peak (dark) or trough (light) daytime cell-muscle correlations. *B*: histogram of latency of peak or trough daytime cell-muscle correlations. *C*: histogram of half-width at half-maximum of narrow correlation component of daytime CCFs. *D*: amplitude of narrow component vs. broad component of daytime CCFs. *E–H*: equivalent plots for nighttime recordings. Bars above histograms indicate mean ±1 SD.

between cell firing rate and simultaneous EMG activity (*monkey Y*: 47 cell-muscle pairs, *monkey K*: 38 cell-muscle pairs). All cells were in the arm and hand area of M1 and all EMG was recorded from contralateral arm and wrist muscles, but no attempt was made to record preferentially from those muscles that were co-activated with cell activity. Most datasets included one wrist flexor and one wrist extensor muscle. Although these muscles were antagonists, the majority of cell-EMG pairs (89%) exhibited a positive correlation around zero-lag, and 29/45 cells exhibited a peak correlation >0.1 with at least one recorded muscle. A histogram of the latencies of the central peak or trough in Fig. 7*B* shows that all features occurred within ±300 ms of zero-lag. The distribution is slightly skewed toward positive latencies (cell leading muscle) with a mean ± SE latency of 22 ± 13 ms, consistent with a causal role for these cells in the generation of movements.

The double Gaussian fits for these cell-muscle CCFs had an average half-width at half-maximum of 840 ± 680 (SD) ms for the narrow component (Fig. 7*C*) and 9.5 ± 10 s for the broad component. Figure 7*D* shows the respective amplitudes of the narrow and broad components for all cell-muscle pairs. The means of these amplitude distributions are similar (narrow: 0.038, broad: 0.033, $P = 0.3$ paired *t*-test), but the SDs were significantly different (narrow: 0.055, broad: 0.030, $P < 0.0001$ *F*-test). This was due in part to negative amplitudes (i.e., troughs) being more common for the narrow component (20%) than for the broad component (4%). There were 13 occurrences of a narrow trough superimposed on a broad peak, but only one case of a narrow peak on a broad trough. This indicates that the majority of cells tend to generally increase firing rate during episodes of active behavior but that within each episode the firing rate may be positively or negatively correlated with specific muscles. For those cell-muscle pairs that exhibited peaks for both narrow and broad components, these amplitudes were positively correlated ($R^2 = 0.36$, $P < 0.0001$).

For the nighttime recordings, the majority of CCFs exhibited a small positive peak. This was true even for those cell-muscle pairs that exhibited a central trough in daytime CCFs (cf. Fig. 4, *A* and *B*). Compared with daytime correlations, the timing of this peak was more variable (Fig. 7*F*) with a latency of 82 ± 69 (SE) ms. The double Gaussian fitting method was used to

further quantify narrow and broad correlation features. The average half-width at half-maximum for these components was respectively 2.3± 1.4 s (Fig. 7*G*) and 47 ± 51 s, both significantly greater than the daytime widths ($P < 0.0001$; paired *t*-test). The amplitudes of narrow and broad components for nighttime CCFs varied independently over a significantly smaller range than for the daytime (Fig. 7*H*).

Neural and muscle recordings during the tracking task

The directional tuning of cells and muscles was assessed from their activity during performance of an isometric two-dimensional (2-D) torque-target tracking task. Figure 8*A* plots the flexion-extension and radial-ulnar components of wrist torque produced during 20 s of this task. These torque components controlled a cursor which the monkey moved from the center hold to one of eight peripheral targets and then held for 1 s. Also shown are rectified EMG traces for muscles ECR and FCU (Fig. 8*B*). Figure 8*C* shows the average rectified EMG profile for each of the eight target directions. The relative EMG level during the peripheral hold period for each target is shown in the polar plots, and the preferred direction for each muscle is consistent with their known actions on the wrist. The CCFs for these antagonist wrist muscles revealed different relationships for the three behavioral conditions. During task performance the muscles were negatively correlated (Fig. 8*D*). The side peaks in this CCF reflect the fact that this animal (*monkey Y*) performed the task at a regular pace with a one complete trial lasting ~3 s. During daytime free behavior the antagonist muscles were positively correlated (Fig. 8*E*). During the night, the muscles were also positively correlated, although the peak of the CCF was smaller and broader than during the day (Fig. 8*F*).

The directional tuning of cortical cells was calculated from PETHs of spike activity aligned to the end of the peripheral hold period. Cell A in Fig. 9 was strongly modulated with torque direction, showing maximal activity when the monkey produced extension torques. CCFs compiled between spike and EMG activity during task performance (Fig. 9*B*) revealed a central correlation peak with the wrist extensor muscle. The width of this peak reflects the temporal profile of task performance, principally determined by the 1-s hold periods. There is

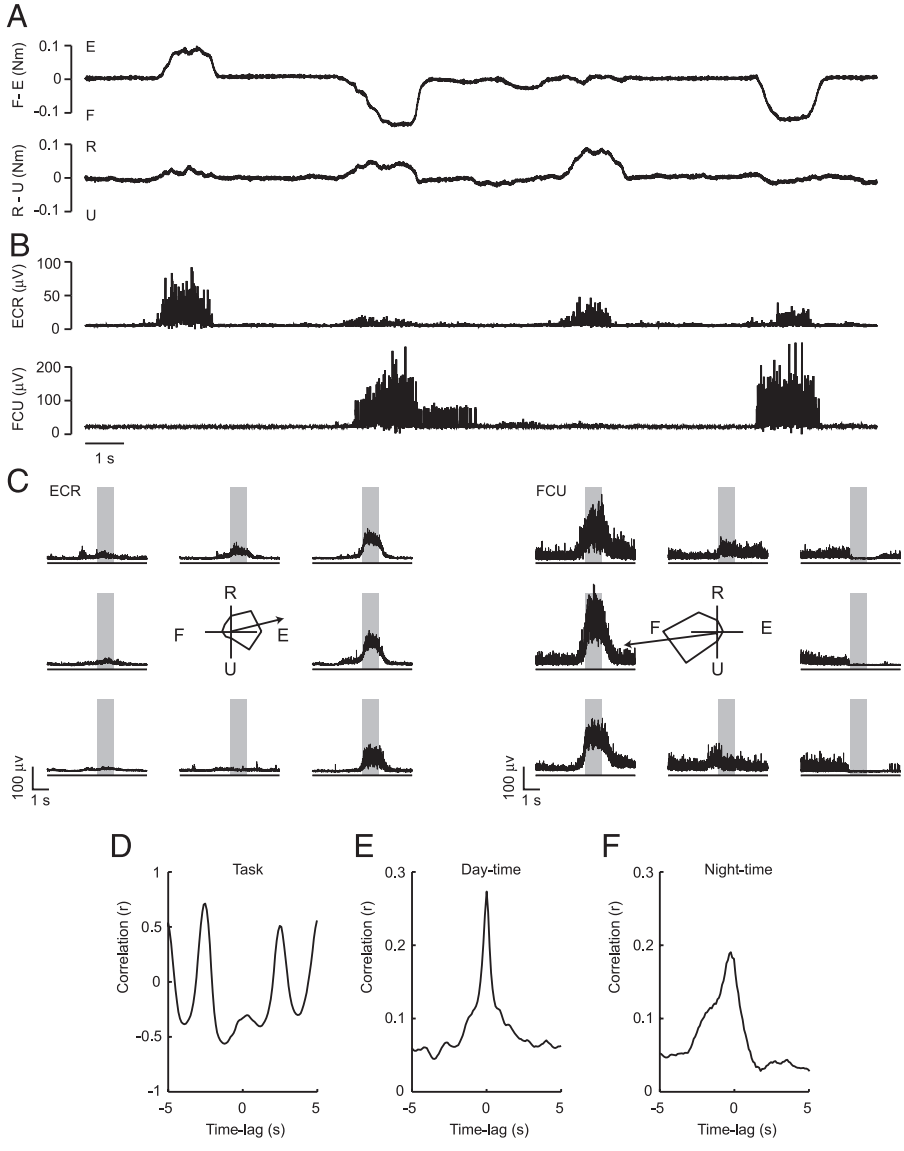

FIG. 8. Recording during the trained task. *A*: wrist torque in the extension (E), flexion (F), radial (R), and ulnar (U) directions as *monkey Y* performed a center-out torque tracking task. *B*: simultaneously recorded rectified EMG from muscles ECR and FCU. *C*: average rectified EMG profiles for the 8 target locations aligned to the hold period (gray shading). Central polar plots show the mean EMG level during the hold period and the preferred direction calculated by vector summation (axes length indicate 100 μV; average of 20 trials per direction). *D*: CCF calculated between ECR and FCU activity over 15 min of task performance. *E*: equivalent CCF for 6 h of daytime free behavior. *F*: equivalent CCF for 6 h of nighttime recording.

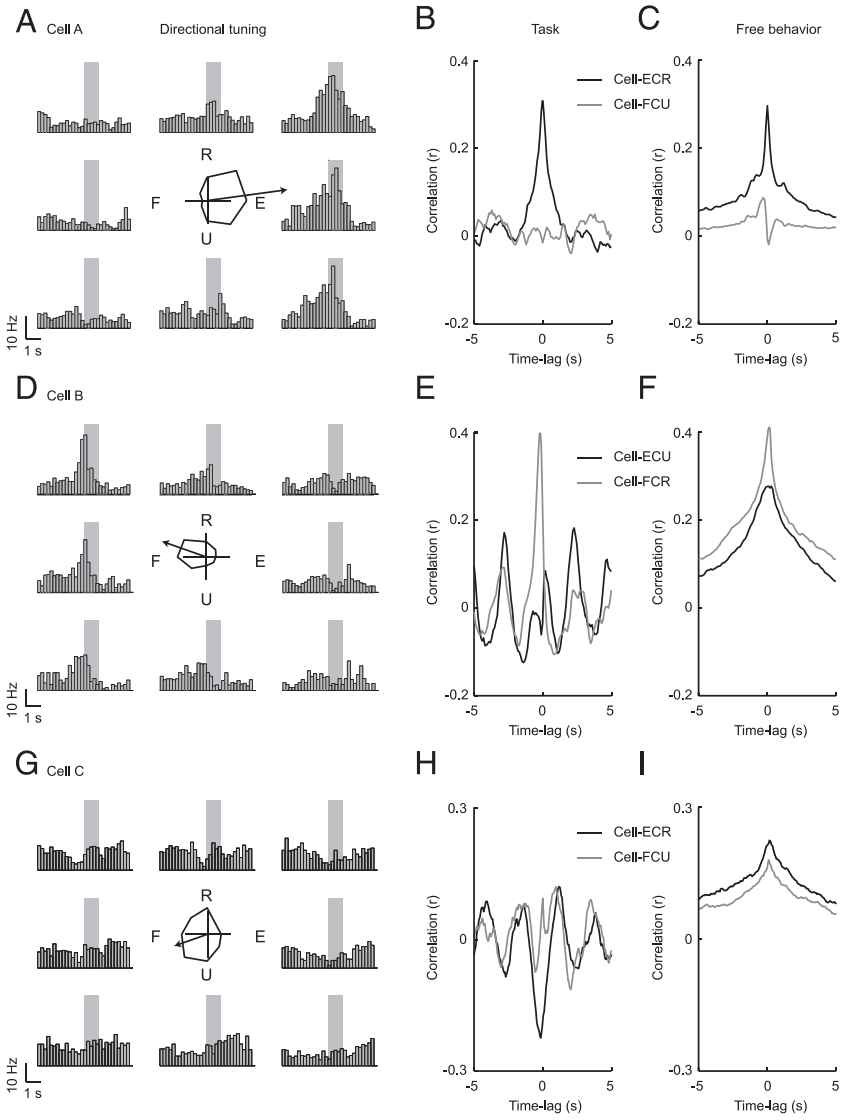

FIG. 9. Comparison of activity during task and free behavior for 3 example cells. *A*: peri-event time histograms (PETHs) of spike activity for the 8 target locations aligned to the peripheral hold period (▨). Central polar plot shows the hold-period firing rate and the preferred direction calculated by vector summation. Cell A (from *monkey K*) showed strong directional tuning with a preference for wrist extension (axes length of polar plot represents 20 Hz; average of 25 trials per direction). *B*: CCFs calculated between cell firing rate and rectified EMG during 30 min of task performance. *C*: CCFs calculated between cell firing rate and rectified EMG during 6 h of daytime free behavior. *D–F*: comparable plots for cell B (*monkey Y*) showing a task preference for flexion. This cell exhibits positive correlations with both flexor and extensor muscles during free behavior. (Analysis based on 10 min of task performance including 12 trials per direction, 7 h of daytime free behavior.) *G–I*: comparable plots for cell C (*monkey Y*) showing weak task modulation. (Analysis based on 10 min of task performance including 12 trials per direction, 4 h of daytime free behavior.)

no broader component to the CCF because the task was performed continuously at a regular pace. CCFs compiled during free behavior (Fig. 9*C*) contain narrow and broad components reflecting the more complex temporal profile of free behavior incorporating episodes of complex activity interspersed with periods of rest. Nevertheless, for this cell CCFs during the task and free behavior were of a similar magnitude; the cell was positively correlated with the extensor muscle and negatively correlated with the flexor muscle over 6 h of unrestrained, daytime activity. Such correspondence between activity during the task and during free behavior was not the case for all cells. Cell B was also modulated with torque direction, with a preference for flexion (Fig. 9*D*). However, this cell exhibited strong positive correlations with both extensor and flexor muscles during free behavior (Fig. 9*F*). Cell C was not strongly modulated with the task (Fig. 9*G*), exhibiting a negative correlation with the wrist extensor (Fig. 9*H*) due to the slight suppression of firing rate for extension torques. In contrast, CCFs compiled during free behavior revealed positive correlation peaks with both extensor and flexor muscles (Fig. 9*I*).

Comparison of cell-muscle correlations during task performance and free behavior

Across all cells there was only a weak relationship between cell-muscle correlation coefficients obtained during the task and during free behavior. Figure 10*A* shows a scatter plot of CCF peaks or troughs for 55 cell-muscle pairs that were recorded during both conditions. The range of coefficients obtained during both conditions was comparable with a maximum cell-muscle correlation during the task of 0.55 compared with 0.41 during free behavior. However, a greater proportion of cell-muscle pairs were negatively correlated during the task (36%) compared with free behavior (9%). The sign of the correlation for 15 cell-muscle pairs was different between conditions, in all cases changing from positive during free behavior to negative during the task. Nevertheless, linear regression yielded a significant relationship between correlation coefficients obtained during the task and free behavior ($R^2 = 0.13$, $P = 0.007$).

Of the two Gaussian components obtained by fitting the free behavior CCFs, only the amplitude of the narrow component was significantly related to the cell-muscle correlation during

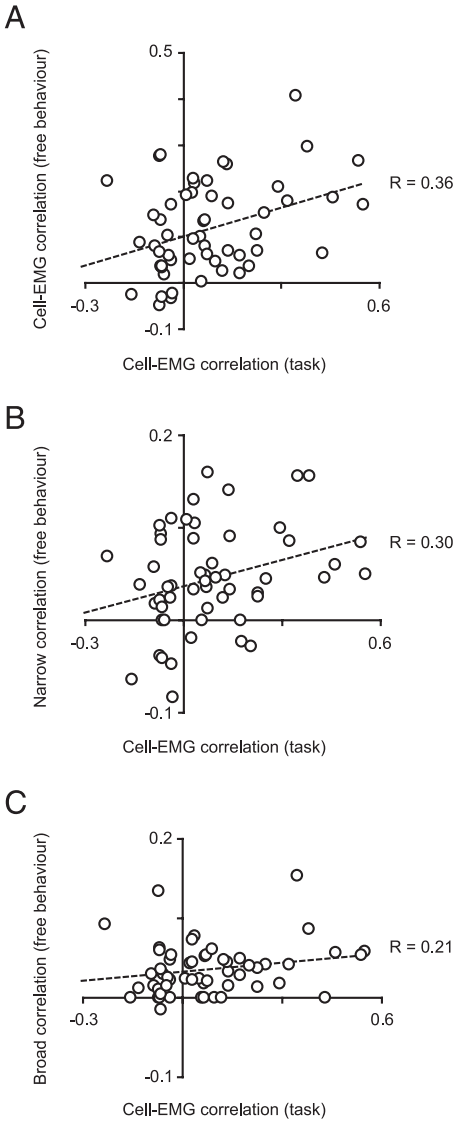

FIG. 10. Comparison of cell-muscle correlations during task and free behavior. *A*: scatter plot of peak (trough) correlation during task vs. free behavior for 55 cell-muscle pairs. *B*: scatter plot of peak (trough) correlation during task vs. amplitude of narrow Gaussian fit component during free behavior. *C*: scatter plot of peak (trough) correlation during task vs. amplitude of broad Gaussian fit component during free behavior.

the task (Fig. 10*B;* $R^2 = 0.09$, $P = 0.03$). For the wide component, the slight positive trend did not reach significance (Fig. 10*C;* $R^2 = 0.04$, $P = 0.14$). There was no significant relationship between cell-muscle correlation values obtained during the task and during nighttime recordings ($R^2 = 0.002$, $P = 0.7$; data not shown).

To investigate the degree to which patterns of cell-muscle correlations during free behavior could be used to predict directional tuning during the task we analyzed 28 cells for which a wrist extensor and a wrist flexor were recorded simultaneously and divided them according to directional preference (extension: 11, flexion: 9, no preference: 8) as determined by activity during the tracking task (see METHODS). In Fig. 11*A*, the peak (trough) cell-flexor muscle correlation coefficient during free behavior is plotted on the vertical axis against the corresponding cell-extensor muscle correlation on the horizontal axis. The cells are color-coded according to directional preference during the task. Three cells with a task preference for flexion fall above the equality line, indicating a stronger correlation with the flexor muscle during free behavior. Six cells with a task preference for extension exhibit stronger correlations with the extensor muscle. However, the scatter plot shows considerable overlap between the three groups and half of the directionally tuned cells fall near the diagonal representing equal correlation with both extensor and flexor. For these cells, CCFs compiled during free behavior would be incapable of predicting directional tuning during the task. Furthermore, four cells exhibited a stronger correlation with the extensor muscle than with the flexor during free behavior but, contrary to expectations, showed no directional preference during the task. In contrast with daytime recordings,

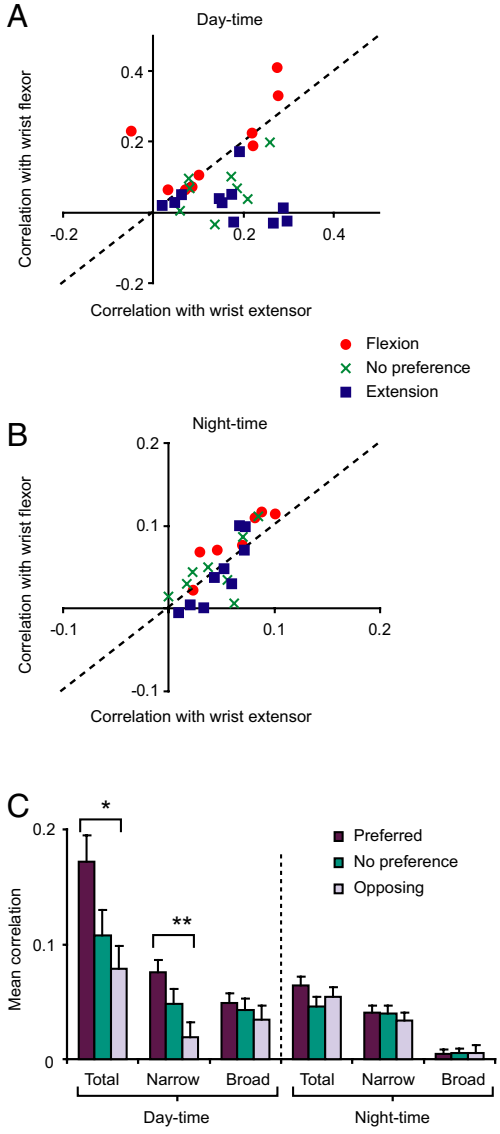

FIG. 11. Relationship between cell-muscle correlations and directional tuning. *A*: scatter plot of peak (trough) correlation with wrist flexor and wrist extensor muscles during daytime free behavior for 28 cells. Cells are coded according to directional preference determined by the trained task. *B*: equivalent plot for nighttime recordings. *C*: average total correlation and amplitude of broad and narrow correlation components, divided for "preferred," "opposing," and "no preference" cell-muscle pairs (see RESULTS). * $P = 0.01$, ** $P = 0.006$.

the cell-muscle correlation values for the nighttime activity show no separation among the three groups of cells defined by task directional preference (Fig. 11*B*). All points fall near the diagonal representing equal correlation with both extensor and flexor muscles. Thus it appears that during the sporadic nighttime movements, the pattern of correlation is less tuned to specific muscles than during the day.

For cells with a significant directional preference for either extension or flexion, we determined the average correlation between firing rate and the muscles acting in the "preferred" and "opposing" directions separately. For cells with no directional preference we combined both flexors and extensors in the "no preference" group. We also analyzed the average contribution of the narrow and broad correlation features for each group as determined by the double Gaussian fit. The results for day- and nighttime activity are summarized in Fig. 11*C*. On average, during the daytime cells were more strongly correlated with muscles acting in their preferred direction than opposing direction. Correlations in the no preference group showed intermediate correlation strengths. This effect of directional preference was significant for the total correlation ($P = 0.01$, 1-factor ANOVA) and the amplitude of the narrow correlation feature ($P = 0.006$) but not the broad feature ($P = 0.5$). During the nighttime, there was no significant effect of directional preference on any of the three correlation measures.

Stability of recordings over several weeks

In some cases we tracked the activity of the same cell over several days to weeks. In agreement with a previous report (Sunner et al. 2005), we found that the preferred directions of cells generally remained stable. In addition, we were able to examine the strength of individual cell-muscle correlations during free behavior over the same periods of time. Figure 12*A* shows spike waveforms for a cell recorded over a 2-wk period from *monkey K*. The preferred direction of this cell, as assessed using the tracking task, was consistent throughout (Fig. 12*B*). Furthermore, the CCF between this cell and the muscle ECR (which acted in the preferred direction) during free behavior remained similar (Fig. 12*C*). Figure 12, *D–F,* shows similar plots for a flexion-tuned cell and muscle FCR from *monkey Y* over a 1-wk period. These recordings demonstrate that the relationship between cell and muscle activity can be stable over long periods of time, even during completely unrestrained behavior.

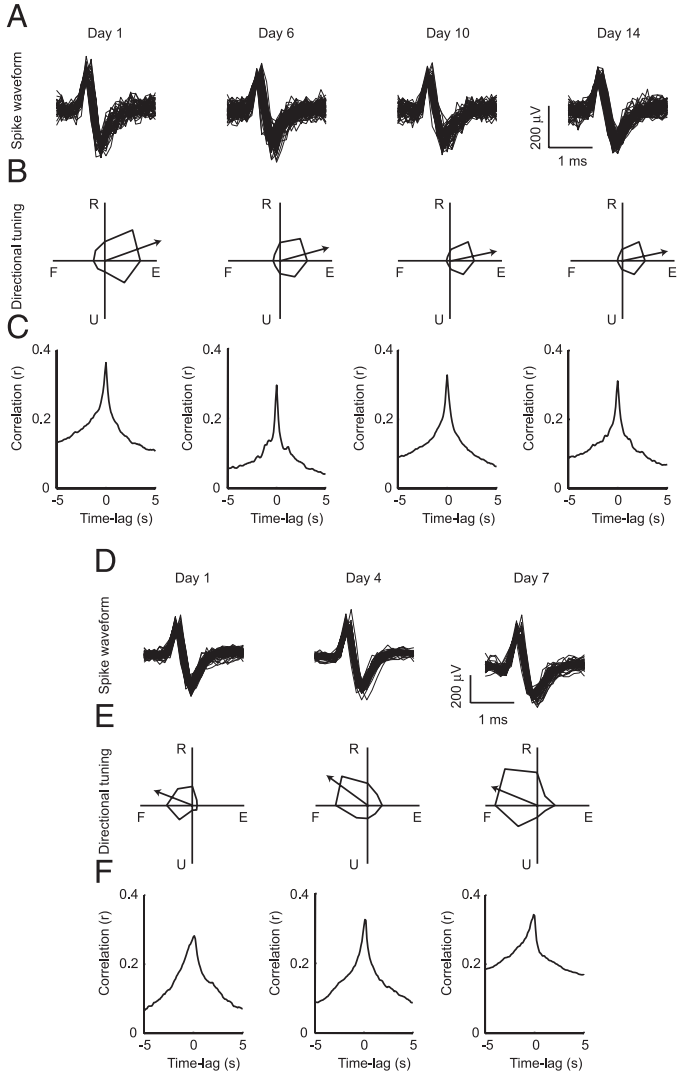

FIG. 12. Stability of neural recordings over 2 wk. *A*: sample spike waveforms recorded during free behavior from *monkey K* over a 2-wk period. *B*: directional tuning calculated as in Fig. 9 for this cell over the same period (~20 trials per direction per day, axes length indicate 40 Hz). *C*: CCFs between cell activity and muscle ECR during daytime behavior over the same period (~6 h per direction per day). *D–F*: waveforms, directional tuning and CCF with muscle FCR for a flexion-tuned cell recorded over a 1-wk period from *monkey Y*.

DISCUSSION

Long-term recording during unrestrained behavior

Using implanted electrodes and an autonomous, battery-powered electronic circuit (the Neurochip), we have for the first time obtained stable, continuous recordings of motor cortex cell activity and muscle EMG in primates during unrestrained behavior and sleep. These results provide a first insight into motor cortex activity under natural conditions. A major finding is that motor cortex cells exhibit high firing rates with strong and consistent correlations with contralateral muscles across long periods of daytime activity. Correlation coefficients of up to $r = 0.4$ were obtained over 6 h of unrestrained behavior; this is only slightly less than the maximum correlation values obtained during performance of a repetitive task. Averaging over a multitude of different behaviors might be expected to diminish considerably the strength of correlations in comparison to those obtained during repetition of a specific movement. Our results instead demonstrate that some motor cortex cells encode a remarkably consistent representation of arm muscle activation across the entire repertoire of natural behavior. Analysis of cell-muscle CCFs revealed two major components: a broad positive correlation reflecting co-variation of cells and muscles over the time scale of movement episodes and a narrow component indicating a temporally precise relationship that we interpret as control of specific muscle synergies within each episode. Interestingly, the majority of cell-muscle pairs exhibited both components, suggesting that precise information about activation of a particular arm muscle can be readily obtained from most cells in the arm area of motor cortex.

Comparison between constrained and unconstrained paradigms

Across the population of cells we recorded, the cell-muscle correlations obtained during free behavior were only weakly related to those obtained while monkeys performed the torque-tracking task. A number of cells exhibited strikingly different patterns of correlation during the two conditions. However, on average cells tended to show stronger correlations with muscles acting in their preferred direction as defined from the task data. These results are broadly consistent with a model in which muscle groups are driven by cortical populations within which individual neurons may exhibit a range of relationships to behavior (Fetz 1992; Todorov 2000). This may account for the apparent diversity of neural representation found in M1 (Scott 2003) including context-dependent coding (Hepp-Reymond et al. 1999; Thach 1978) and different neuronal subsystems for controlling posture and movement (Kurtzer et al. 2005).

The dependence on preferred direction was significant only for the narrow cross-correlation component, supporting our interpretation that this feature reflects control of specific muscle groups within each behavioral episode. However, it should be noted that those cells that exhibited no directional tuning in the wrist task could nevertheless be positively correlated with wrist muscles during free behavior, and even correlations with muscles opposing the preferred direction of tuned cells were on average positive during free behavior. This counter-intuitive finding may result from the synergistic involvement of many muscles during natural movement, which includes frequent co-contraction of antagonists. This illustrates a major difference between free behavior and the performance of an artificial task. In traditional studies of motor control, limiting the range of motion has been necessary for stable cell recording, but constrained paradigms also offer a methodological advantage by isolating the activity of specific groups of muscles. However, this approach thereby imposes an artificial pattern of muscle use (e.g., Fig. 8, *D* vs. *E*) and can provide only a limited insight into the control of natural, coordinated movements. For instance, cell C documented in Fig. 9 exhibited no directional preference in the wrist task but may have controlled a specific synergy of muscles that was not represented in the restricted task. Many corticomotoneuronal cells that produce postspike facilitation in both proximal and distal muscles are preferentially activated during movements that coactivate their target muscles (McKiernan et al. 1998). Alternatively, this cell may simply have controlled proximal muscles that tended to be used in synergy with wrist muscles. As recordings from more muscles during free behavior become technically feasible it should be possible to resolve these issues.

Several other factors could also explain the discrepant relationships we observed between task performance and free behavior. Learned movements typically involve a different pattern of muscle activity compared with novel volitional movements (Thoroughman and Shadmehr 1999), and the extensive repetition necessary for behavioral training may affect the representation of specific movements within motor cortex (Nudo et al. 1996). Another factor may be the range of activity levels sampled. During our task, maximum cortical firing rates, even for preferred directions, were in the range of 40–80 Hz. However, during free behavior, instantaneous firing rates during a single 100-ms bin regularly exceeded 100–200 Hz (interspersed raw samples showed no evidence of cell injury or multi-unit discharge). Peak EMG levels were correspondingly higher. This suggests that free behavior includes episodes of greater activity than are normally incorporated into repetitive tasks requiring only a fraction of maximum voluntary contraction. Whatever the explanation of the differences between constrained and unconstrained paradigms, our present results suggest that neither approach alone can provide a complete description of the relationship between individual cortical cells and the movements they encode.

Relevance to neuromotor prosthetics

The development of neural prosthetics provides further motivation for expanding the application of electrophysiological recording techniques beyond constrained paradigms. Recent years have seen renewed interest in the possibility of using movement information extracted from cortical recordings to restore function in patients with motor deficits (Donoghue 2002). To date, neuromotor prosthetics have been limited to control of cursors or simple robotic arms (Carmena et al. 2003; Hochberg et al. 2006; Serruya et al. 2002; Taylor et al. 2002), but in the future, motor cortex spike activity could be used to control spinal cord microstimulation (Jackson et al. 2006a; Mushahwar et al. 2000) or functional neuromuscular stimulation (Keith et al. 1988) to move the patient's own limbs. Our results suggest that extracting muscle activation patterns from cortical activity could help restore a more complete range of motor behavior than previously thought. The strong correlations we found between individual cells and muscle activity and the long-term stability of these relationships bode well for the success of neuromotor prosthetics. The temporally precise cortex-muscle relationship revealed by the narrow cross-correlation component, which also reflected directional preference during the task, would presumably be useful for control of a prosthesis. During repetitive tasks, linear combinations of the activity of multiple cells yield improved prediction of muscle patterns (Carmena et al. 2003; Morrow and Miller 2003; Santucci et al. 2005; Westwick et al. 2006), although the extent to which this will generalize to unrestricted movements remains to be seen. In addition, the broad cross-correlation peaks we observed suggest that a measure of the overall level of activity within a population of cells could provide a reliable ON-OFF signal to indicate periods of intended behavior.

Nighttime correlations between cortex and muscles

We found that during the night motor cortex cells often exhibited regular periods of high firing rate. Elevated motor cortical activity associated with REM sleep has been described previously in chaired monkeys (Evarts 1964) and the time course of the cycles in our data is consistent with previous electroencephalogram (EEG) and behavioral studies of macaque sleep (Balzamo et al. 1998; Weitzman et al. 1965). Although at present we are unable to record simultaneous field potentials with our Neurochip system, the periods of elevated cortical activity presumably correspond to periods of desynchronized EEG. The highest firing rates were comparable to daytime values but associated with complete atonia, characteristic of REM sleep. Atonia arises from inhibition of motoneu-

rons by brain stem structures, and is enhanced during REM, possibly to balance increased descending excitation (Chase and Morales 1990; Steriade and Hobson 1976). Interestingly, we observed that nighttime EMG activity occurred predominantly during the transitions into and out of each phase of elevated cortical activity and may have been associated with light sleep or waking. One possible explanation for this pattern is that the periods of elevated cortical activity and spinal inhibition do not completely overlap. A recent study in rats (Lu et al. 2006) has found separate populations of neurons in the brain stem mediating atonia and cortical EEG patterns during REM, which may allow this dissociation. Our results suggest that the period of enhanced spinal inhibition begins slightly after and ends slightly before the period of high cortical activity. Such a mismatch could explain the predominance of apparent waking episodes just before or after REM sleep in macaques (Balzamo et al. 1998; Weitzman et al. 1965).

The functional role of REM activity, and sleep in general, is the subject of considerable debate (e.g., Siegel 2005; Stickgold and Walker 2005). It has been suggested that during development, twitching in sleep contributes to the organization spinal reflex circuitry (Petersson et al. 2003). Sleep may be important for consolidation of motor learning (Fischer et al. 2002; Walker et al. 2005) although this hypothesis remains controversial (Vertes 2004). The pattern of cortex-muscle correlations we saw during the night clearly differed from that during daytime recordings. The strength of correlation varied through the sleep cycle, consistent with a fluctuating level of spinal inhibition. Cell-muscle correlations were slightly wider and generally positive during periods of movement, in contrast to the mix of narrow correlation peaks and troughs seen during the day. Most notably, the directional tuning of cells was no longer reflected in correlation coefficients for pairs of antagonist muscles and cell activity could be correlated with both contra- and ipsilateral muscles. These observations suggest that widespread synchronous bursts of cortical activity during sleep, possibly extending across both hemispheres, leads to less specificity in the pattern of correlation between individual cell-muscle pairs. On average, cortical firing led muscle activity, but there was a wider range of large positive and negative time lags compared with daytime recordings, indicating that these correlations may not be mediated only by direct corticospinal pathways, and possibly include a contribution from co-excitation by a common brain stem drive (Marchiafava and Pompeiano 1964; Steriade and Hobson 1976).

One further point relevant to the use of cortical activity to control a prosthesis or functional electrical stimulation is that the periods of highest cell activity during the night coincide with descending inhibition of motoneurons. Any artificial link bypassing this physiological inhibition could generate uncontrolled movements so would need to be shut off if the user fell asleep.

Conclusions

The use of chronic electrodes and autonomous, implantable electronics can significantly extend the scope of electrophysiological research into natural behavior. We have shown that stable, long-term motor cortex and muscle recordings can be obtained from primates during completely unrestrained behavior and that this data complement recording during a conventional constrained task. Cells and muscles were followed through the repertoire of natural movements and sleep, providing a first glimpse of activity within the motor system during normal behavior. Although patterns of correlation for individual cells could differ between conditions, the overall correspondence within our results supports the tacit assumption underlying many previous experiments that data obtained under restrained conditions can be more broadly informative of the neural control of natural movements. Furthermore, the ability to record the same cells continuously for several weeks opens up new possibilities for studying neural control of complex behaviors and motor learning (Jackson et al. 2006b). Finally, linking autonomously recorded cell activity to functional electrical stimulation may lead to the development of neural prosthetics to restore volitional motor function after injury.

ACKNOWLEDGMENTS

We thank C. Kirby, J. Longnion, and L. Shupe for technical assistance and S. Perlmutter for advice.

GRANTS

This work was supported by the National Institutes of Health Grants NS-12542 and RR-00166, Office of Naval Research Grant N00014-01-1-0676, and the University of Washington Royalty Research Fund.

REFERENCES

Aflalo TN, Graziano MS. Partial tuning of motor cortex neurons to final posture in a free-moving paradigm. *Proc Natl Acad Sci USA* 103: 2909–2914, 2006.

Balzamo E, Van Beers P, Lagarde D. Scoring of sleep and wakefulness by behavioral analysis from video recording in rhesus monkeys: comparison with conventional EEG analysis. *Electroencephalogr Clin Neurophysiol* 106: 206–212, 1998.

Caminiti R, Johnson PB, Urbano A. Making arm movements within different parts of space: dynamic aspects in the primate motor cortex. *J Neurosci* 10: 2039–2058, 1990.

Carmena JM, Lebedev MA, Crist RE, O'Doherty JE, Santucci DM, Dimitrov DF, Patil PG, Henriquez CS, Nicolelis MA. Learning to control a brain-machine interface for reaching and grasping by primates. *PLoS Biol* 1: E42, 2003.

Chase MH, Morales FR. The atonia and myoclonia of active (REM) sleep. *Annu Rev Pschol* 41: 557–584, 1990.

Cheney PD, Fetz EE. Functional classes of primate corticomotoneuronal cells and their relation to active force. *J Neurophysiol* 44: 773–791, 1980.

Donoghue JP. Connecting cortex to machines: recent advances in brain interfaces. *Nat Neurosci* 5: 1085–1088, 2002.

Evarts EV. Temporal patterns of discharge of pyramidal tract neurons during sleep and waking in the monkey. *J Neurophysiol* 27: 152–171, 1964.

Evarts EV. Relation of pyramidal tract activity to force exerted during voluntary movement. *J Neurophysiol* 31: 14–27, 1968.

Fetz EE. Are movement parameters recognizably coded in the activity of single neurons? *Behav Brain Sci* 15: 679–690, 1992.

Fischer S, Hallschmid M, Elsner AL, Born J. Sleep forms memory for finger skills. *Proc Natl Acad Sci USA* 99: 11987–11991, 2002.

Georgopoulos AP, Kalaska JF, Caminiti R, Massey JT, On the relations between the direction of two-dimensional arm movements and cell discharge in primate motor cortex. *J Neurosci* 2: 1527–1537, 1982.

Hepp-Reymond MC, Kirkpatrick-Tanner M, Gabernet L, Qiao J, Weber B. Context-dependent force coding in motor and premotor cortices. *Exp Brain Res* 128: 123–133, 1999.

Hochberg LR, Serruya MD, Friehs GM, Mukand JA, Saleh M, Caplan AH, Branner A, Chen D, Penn RD, Donoghue JP. Neuronal ensemble control of prosthetic devices by a human with tetraplegia. *Nature* 442: 164–171, 2006.

Holdefer RN, Miller LE. Primary motor cortical neurons encode functional muscle synergies. *Exp Brain Res* 146: 233–243, 2002.

Hoogerwerf AC, Wise KD. A three-dimensional microelectrode array for chronic neural recording. *IEEE Trans Biomed Eng* 41: 1136–1146, 1994.

Jackson A, Mavoori J, Longnion J, Fetz EE. Motor cortex and muscle activity in freely behaving primates documented with an implanted brain-computer interface. *Soc Neurosci Abstr* 402.3, 2005.

Jackson A, Moritz CT, Mavoori J, Lucas TH, Fetz EE. The Neurochip BCI: toward a neural prosthesis for upper limb function. *IEEE Trans Neural Sys Rehab Eng* 14: 187–190, 2006a.

Jackson A, Mavoori J, Fetz EE. Long-term motor cortex plasticity induced by an electronic implant. *Nature* 2006b.

Keith MW, Peckham PH, Thorpe GB, Buckett JR, Stroh KC, Menger V. Functional neuromuscular stimulation neuroprostheses for the tetraplegic hand. *Clin Orthop* 233: 25–33, 1988.

Kralik JD, Dimitrov DF, Krupa DJ, Katz DB, Cohen D, Nicolelis MA. Techniques for chronic, multisite neuronal ensemble recordings in behaving animals. *Methods* 25: 121–150, 2001.

Kurtzer I, Herter TM, Scott SH. Random changes in cortical load representation suggest distinct control of posture and movement. *Nat Neurosci* 8: 498–504, 2005.

Lemon RN. Methods for neuronal recording in conscious animals. In: *IBRO Handbook Series: Methods in Neurosciences* 4, edited by AD Smith. London: Wiley, 1984, p. 1–162.

Lu J, Sherman D, Devor M, Saper CB. A putative flip-flop switch for control of REM sleep. *Nature* 441: 589–594, 2006.

Marchiafava PL, Pompeiano O. Pyramidal influences on spinal cord during desynchronized sleep. *Arch Ital Biol* 102: 500–529, 1964.

Mavoori J, Jackson A, Diorio C, Fetz EE. An autonomous implantable computer for neural recording and stimulation in unrestrained primates. *J Neurosci Methods* 148: 71–77, 2005.

McKiernan BJ, Marcario JK, Karrer JH, Cheney PD. Corticomotoneuronal postspike effects in shoulder, elbow, wrist, digit, and intrinsic hand muscles during a reach and prehension task. *J Neurophysiol* 80: 1961–1980, 1998.

Moran DW, Schwartz AB. Motor cortical representation of speed and direction during reaching. *J Neurophysiol* 82: 2676–2692, 1999.

Morrow MM, Miller LE. Prediction of muscle activity by populations of sequentially recorded primary motor cortex neurons *J Neurophysiol* 89: 2279–2288, 2003.

Mushahwar VK, Collins DF, Prochazka A. Spinal cord microstimulation generates functional limb movements in chronically implanted cats. *Exp Neurol* 163: 422–429, 2000.

Nordhausen CT, Maynard EM, Normann RA. Single unit recording capabilities of a 100 microelectrode array. *Brain Res* 726: 129–140, 1996.

Nudo RJ, Milliken GW, Jenkins WM, Merzenich MM. Use-dependent alterations of movement representations in primary motor cortex of adult squirrel monkeys. *J Neurosci* 16: 785–807, 1996.

Petersson P, Waldenstrom A, Fahraeus C, Schouenborg J. Spontaneous muscle twitches during sleep guide spinal self-organization. *Nature* 424: 72–75, 2003.

Santucci DM, Kralik JD, Lebedev MA, Nicolelis MA. Frontal and parietal cortical ensembles predict single-trial muscle activity during reaching movements in primates. *Eur J Neurosci* 22: 1529–1540, 2005.

Scott SH. The role of primary motor cortex in goal-directed movements: insights from neurophysiological studies on non-human primates. *Curr Opin Neurobiol* 13: 671–677, 2003.

Serruya MD, Hatsopoulos NG, Paninski L, Fellows MR, Donoghue JP. Instant neural control of a movement signal. *Nature* 416: 141–142, 2002.

Siegel JM. Clues to the function of mammalian sleep. *Nature* 437: 1264–1271, 2005.

Steriade M, Hobson JA. Neuronal activity during the sleep-waking cycle. *Prog Neurobiol* 6: 157–376, 1976.

Stickgold R, Walker MP. Sleep and memory: the ongoing debate. *Sleep* 28: 1225–1226, 2005.

Sunner S, Fellows MR, Vargas-Irwin C, Nakata GK, Donoghue JP. Reliability of signals from a chronically implanted, silicon-based electrode array in non-human primate primary motor cortex. *IEEE Trans Neural Sys Rehab Eng* 13: 524–541, 2005.

Taylor DM, Tillery SI, Schwartz AB. Direct cortical control of 3D neuroprosthetic devices. *Science* 296: 1829–1832, 2002.

Thach WT. Correlation of neural discharge with pattern and force of muscle activity, joint position and direction of intended next movement in motor cortex and cerebellum. *J Neurophysiol* 41: 654–676, 1978.

Thoroughman KA, Shadmehr R. Electromyographic correlates of learning an internal model of reaching movements. *J Neurosci* 19: 8573–8588, 1999.

Todorov E. Direct cortical control of muscle activation in voluntary arm movements: a model. *Nat Neurosci* 3: 391–398, 2000.

Townsend BR, Paninski L, Lemon RN. Linear encoding of muscle activity in primary motor cortex and cerebellum. *J Neurophysiol* 96: 2578–2592, 2006.

Vertes RP. Memory consolidation in sleep: dream or reality. *Neuron* 44: 135–148, 2004.

Walker MP, Stickgold R, Alsop D, Gaab N, Schlaug G. Sleep-dependent motor memory plasticity in the human brain. *Neuroscience* 133: 911–917, 2005.

Weitzman ED, Kripke DF, Pollak C, Dominguez J. Cyclic activity in sleep of *Macaca mulatta. Arch Neurol* 12: 463–467, 1965.

Westwick DT, Pohlmeyer EA, Solla SA, Miller LE, Perreault EJ. Identification of multiple-input systems with highly coupled inputs: application to EMG prediction from multiple intracortical electrodes. *Neural Comput* 18: 329–355, 2006.